第32卷 第2期 焊 接 学 报 Vol.32 No.2
2011年2月 TRANSACTIONS OF THE CHINA WELDING INSTITUTION February 2011

盲孔法中应变释放系数的有限元模拟标定

马雯波[1,2], 陈曙光[2], 刘荟琼[2], 林 稳[2], 沈玉龙[1], 刘吉普[1]

(1. 湘潭大学 机械工程学院, 湘潭 411105;
2. 湖南省特种设备检测中心, 长沙 410000)

马雯波

摘 要: 盲孔法测量焊接残余应力时,孔周围材料超过屈服状态,产生塑性变形而引入塑性附加应变,使得测量结果产生较大误差. 根据应变释放系数 A, B试验标定原理,对 Q345R钢进行试验标定. 以一定应力状态下形状改变比能系数 S作为判据,对应变释放系数 A, B进行修正,使得焊接等高残余应力的测量结果更为精确. 基于强度理论,应用有限元软件,对 Q345R钢的应变释放系数 A, B进行三维有限元数值计算. 结果表明,用有限元进行应变释放系数的塑性修正是可行的.

关键词: 盲孔法; 焊接残余应力; 应变释放系数; 标定试验; 有限元法
中图分类号: TG404 文献标识码: A 文章编号: 0253-360X(2011)02-0097-04

0 序 言

盲孔法是德国学者 Mathar于 1934年提出,后经 Soete和 Vancombrugge等学者的发展,测量精度大为提高. 它具有操作简单、测量方便、对构件损伤程度小等特点. 根据 ASTM标准 E837[1]生产的残余应力应变片 TJ120-1.5Φ1.5,其 A, B值的标定只停留在传统的标定方法下,当残余应力值超过二分之一材料屈服强度时,其测量误差较大,有时超过 20%. 高残余应力测量中,总应变包括因钻削加工引起的塑性变形、纯弹性释放应变和应力集中引起的塑性应变. 对钻削加工塑性应变可以通过在无应力试板上钻孔测得,而对于孔边应力集中塑性应变的修正方法主要有:通过拉伸试验,得出材料应变释放系数塑性修正曲线[2],作出基于孔边形状改变比能参量 S的应变释放系数塑性修正公式[3];以及迭代修正法[4]和应变释放系数分级使用法[5]等. 通过对试件进行大标定试验,获得有孔边塑性变形的 A, B值;用修正后的 A, B系数来抵消附加应变. 利用 ANSYS软件,建立三维有限元模型,模拟标定试验. 将两者的标定结果进行对比,获得比较可靠的 A, B值.

1 盲孔法测量残余应力的基本原理

若构件内存在残余应力场和应变场,在应力场内任意点钻一小盲孔,该处金属的残余应力即被释放,盲孔周围将产生一定量的释放应变,使应力场达到新的平衡,形成新的应力场和应变场,测出释放应变,即可利用相应公式计算出该测试点的初始残余应力.

目前关于盲孔法测量残余应力的计算公式是建立在通孔法的基础上. 对于由图 1所示应变片测得的释放应变,其应力计算公式为

$$\left.\begin{aligned}\sigma_{1,2}&=\frac{\varepsilon_1+\varepsilon_2}{4A}\mp\frac{1}{4B}\sqrt{(\varepsilon_1-\varepsilon_3)^2+(2\varepsilon_2-\varepsilon_1-\varepsilon_3)^2}\\ \tan 2\theta&=\frac{2\varepsilon_2-\varepsilon_1-\varepsilon_3}{\varepsilon_3-\varepsilon_1}\end{aligned}\right\}\quad(1)$$

式中: A, B为应变释放系数; ε为应变.

应变释放系数 A和 B则需由标定试验确定. 假设人为地在构件中施加单向应力场($\sigma_1=\sigma$, $\sigma_2=0$),应变片 R_1, R_3分别平行于 σ_1, σ_2方向,即 $\gamma=0$,代入式(1)则有

$$\left.\begin{aligned}\sigma_1&=\frac{\varepsilon_1+\varepsilon_3}{4A}+\frac{\varepsilon_1-\varepsilon_3}{4B}\\ \sigma_2&=\frac{\varepsilon_1+\varepsilon_3}{4A}-\frac{\varepsilon_1-\varepsilon_3}{4B}\end{aligned}\right\}\quad(2)$$

将单向应力场代入式(2)可得

$$\left.\begin{aligned}A&=(\varepsilon_1+\varepsilon_3)/2\sigma\\ B&=(\varepsilon_1-\varepsilon_3)/2\sigma\end{aligned}\right\}\quad(3)$$

释放应变 ε_1, ε_3由应变片 R_1, R_3测得,从而可求出应变释放系数 A, B.

收稿日期: 2009-10-09
基金项目: 湖南省特种设备检测中心基金资助项目(07KH/KH01049)

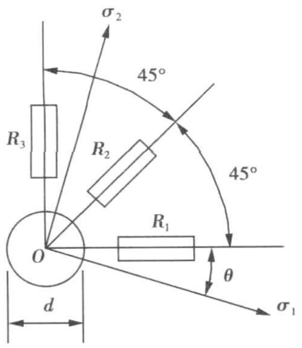

图 1 应变片布置图
Fig. 1 Arrangement of residual strain gauge

2 试验标定方法及试件

标定试验是在特定试件上预先粘贴好应变片，并对试件施加单向载荷，再在试件上钻一定深度的盲孔，通过应变仪记录应变片钻孔前后应变变化(即释放应变)，由式(3)推算出应变释放系数 A，B.

试件采用 Q345R 钢，厚度为 14 mm，根据标准在板材扎制方向 1/4 处取样. 经拉伸试验，得到此批板材的力学性能(表 1). 钻孔直径 1.5 mm，孔深 2 mm. 按图 2 所示贴好应变片，在试件的两侧粘贴校正加载偏心和试件扭转的应变片(监视片).

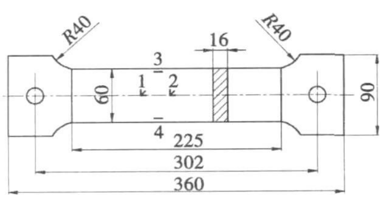

图 2 标定试件及应变片布置
Fig. 2 Specimen and distribution of strain gauge

表 1 板材力学性能
Table 1 Mechanical properties of steel Q345R

钢号	板厚 δ/mm	弹性模量 E/MPa	抗拉强度 R_m/MPa	屈服强度 R_{eL}/MPa	断后伸长率 A(%)
Q345R	14	2.1×10^5	540	345	31

3 弹性段标定试验与结果

根据弹性力学理论，在无限大平板开圆孔，受单向拉伸作用孔边应力集中系数为 3. 为避免孔边产生塑性变形，保证试件在弹性范围内反复加载，拉伸时保证工作部分最大载荷引起的实际应力不大于 1/3 R_{eL}. 在试件中心线上选取一点贴上应变片，选取加载等级为 F=18，36，54，72，90 kN，分别记录下所对应的应变值；钻孔后，将试件再次加载到前述的 5 个 F 值，得到相同应力状态下钻孔前后的应变差值. 再按上述方法，在试件中心线上与前述的测点距离≥25 mm 处选取两点进行加载，记录所对应的应变值. 得到三组数据的误差均≤5%，三次测量监视片的读数偏差亦≤5%. 将此三组数据取平均值，经弯曲、扭转校正和误差修正后，钻孔前后应变差值和对应的 A，B 系数值见表 2.

表 2 弹性状况下标定试验结果
Table 2 Calibration results under elastic state

序号	标定应力 $\sigma_标$/MPa	释放应变 $\triangle\varepsilon_1$	释放应变 $\triangle\varepsilon_3$	应变释放系数 A/($\mu\varepsilon\cdot MPa^{-1}$)	应变释放系数 B/($\mu\varepsilon\cdot MPa^{-1}$)
1	21	−24	9	−0.352 15	−0.774 72
2	43	−50	19	−0.361 26	−0.804 10
3	64	−71	30	−0.319 78	−0.787 75
4	86	−98	38	−0.350 44	−0.794 33
5	107	−120	45	−0.350 23	−0.770 52

由表 2 可得到在常规标定下，$A=-0.346\,77\times10^{-6}$，$B=-0.786\,28\times10^{-6}$.

然后逐步增加载荷，一直增加到接近屈服极限 R_{el} 为止，得出相应的应力应变值. 通过式(3)，计算出相应的应变释放系数 A，B 值.

4 有限元法标定

4.1 计算模型

由于试件具有对称性，取标定试件中间部分的 1/4 建立 ANSYS 有限元模型，网格划分见图 3. 采用线性强化弹塑性模型，材料的应力应变曲线如图 4 所示，其弹性模量为 $E=2.1\times10^5$ MPa，泊松比 $\upsilon=0.3$，屈服强度 $R_{eL}=345$ MPa，服从各向同性强

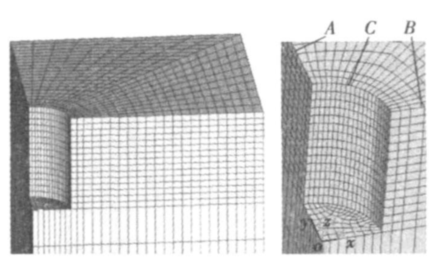

(a) 模型的网格划分 (b) 盲孔附近的网格划分

图 3 有限元网格划分
Fig. 3 Picture of element division

化，采用 Mises屈服准则．整个模型均为六面体单元，受方向均匀载荷 F作用．F逐步增加一直达到材料的屈服极限值为止．

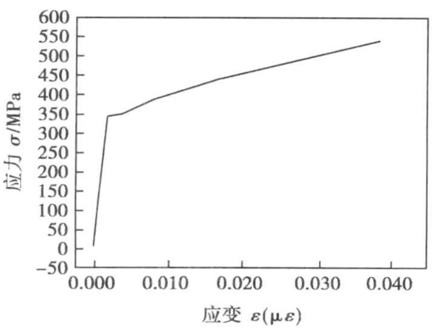

图 4　Q345R拉伸应力－应变曲线

Fig. 4　Stress_strain curves of Q345R

4.2　边界条件处理

由于具有对称性，在 YOZ面上所有节点的 x方向位移为 0，在 XOZ面上所有节点的 y方向位移为 0，为避免模型结构奇异性，令节点（0，0，0）的位移为 0．

4.3　钻孔引起加工硬化的有限元模拟

为了真实模拟释放系数的测定试验，应考虑钻孔后孔边附近产生的加工硬化，建立有限元模型，使数值计算的结果更加接近实际[6]．在应变片位置，按照敏感栅的形状和大小划分网格（图 3 b中的 A，B矩形区域），在钢材上钻孔时的平均加工硬化深度为 0.18～0.2 mm，为此，在盲孔边缘取 0.2 mm厚作为加工硬化层，划分环形单元（图 3 b中的 C区域）．

5　有限元塑性修正

根据弹塑性力学理论，当单向拉伸载荷大于 $R_{eL}/3$时，孔边产生塑性变形，由上述方法标定得到应变释放系数 A，B，不再是与应力大小无关的常量．为确定孔边塑性变形引起的误差大小，用有限元模型进行大应力标定试验模拟，加载等级为 F＝115～345 MPa．获得钻孔前后应变与应力的关系（图 5），当应力＜0.42 R_{eL}时，钻孔后应变与应力水平基本呈线性关系，当应力＞0.42 R_{eL}时，应变偏差量随 σ/R_{eL}的增大显著增大．

根据强度理论，在平面应力状态下有

$$R_{eL}^2=\sigma_1^2+\sigma_2^2-\sigma_1\sigma_2 \qquad (4)$$

式中：R_{eL}为屈服强度．

考虑到广义胡克定律则有

$$\varepsilon_1=(\sigma_1-\upsilon\sigma_2)/E \qquad \varepsilon_2=(\sigma_2-\upsilon\sigma_1)/E$$

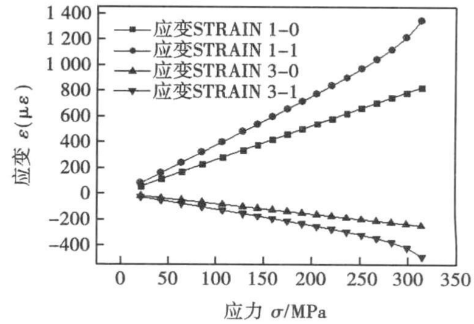

图 5　应变与应力水平关系

Fig. 5　Relationship between stress and strain

式（4）右端可写为

$$\sigma_1^2+\sigma_2^2-\sigma_1\sigma_2=S[E/(1-\upsilon^2)]^2 \qquad (5)$$

$$S=(1-\upsilon^2-\upsilon)(\varepsilon_1^2+\varepsilon_2^2)-(1-\upsilon^2-4\upsilon)\varepsilon_1\varepsilon_2 \qquad (6)$$

式中：ε_1，ε_2分别对应于图 1中的 R_1，R_3；υ为泊松比．

结合形状改变比能理论，可知 S反映了相应应力状态下形状改变比能的大小．由标定试验，可得到应力 σ和 S的关系，如图 6所示．随着应力的增加，S也随之升高，且呈近似指数规律．

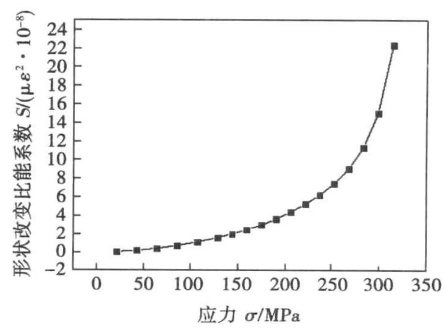

图 6　应力与形状改变比能系数的关系

Fig. 6　Relationship between stress and energy parameter

应变释放系数 A，B和参量 S的关系，如图 7所示．由图可知，应变释放系数 A基本保持不变；S较小时，B随参量 S的变化不明显，当 S大于一定值时，B随 S近似呈线性变化．以形状改变比能的大小 S来作为判据，得到如下修正公式，即

$$A=\begin{cases}-0.341\,163 & S\leqslant 2.0\\ -0.005\,223\times S-0.330\,356 & S>2.0\end{cases} \qquad (7)$$

$$B=\begin{cases}-0.763\,261 & S\leqslant 2.0\\ -0.021\,952\,6\times S-0.719\,503 & S>2.0\end{cases} \qquad (8)$$

将有限元分析得到的应变释放系数 A，B值与实际标定试验所得到的 A，B值进行对比，如图 8所

示,发现两者具有较好的重合性. 考虑到试验标定时存在钻孔偏差、拉伸试板存在微量弯矩等因素的影响. 建议用有限元标定结果作为对高残余应力测量的修正. 利用修正公式对标定试验的结果进行修正,如表 3所示.

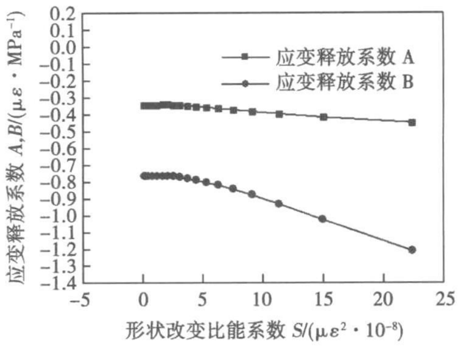

图 7 形状改变比能系数与应变释放系数的关系

Fig. 7 Relationship between energy parameter and strain release factors

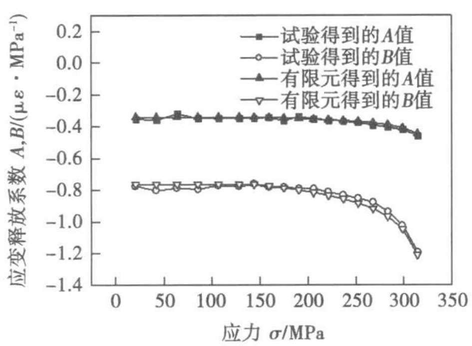

图 8 试验标定值与有限元标定值的对比

Fig. 8 Comparison between test calibration values and finite element calibration values

表 3 修正前后的误差比较

Table 3 Comparison between before and after corrected errors

真实应力 σ/MPa	参量 $S/(\mu\varepsilon \cdot 10^{-8})$	修正应力 σ′/MPa	修正后的相对偏差 R_{SD}(%)	未修正应力 σ″/MPa	未修正的相对偏差 R_{SD}''(%)
143 8	2. 004 17	143. 8	−0. 03%	143 8	−0 03%
159. 3	2. 482 16	158. 3	−0. 62%	159. 9	0 39%
190 3	3. 662 86	187. 4	−1. 55%	194 1	2 01%
205 8	4. 393 35	202. 0	−1. 85%	212 5	3 27%
236 8	6. 240 52	231. 6	−2. 18%	253 1	6 86%
252 3	7. 484 44	247. 1	−2. 08%	276 6	9. 62%
283 3	11. 323 40	279. 9	−1. 18%	336 9	18 91%
298 8	14. 986 00	298. 1	−0. 24%	382 7	28 09%
314 3	22. 368 50	314. 3	0. 00%	455 2	44 84%

经塑性修正公式修正后,最大偏差只有 2. 18%,与未修正的最大偏差 44. 84%相比,误差大大缩小.

6 结 论

(1) 在一定形状改变比能参数下,应变释放系数几乎是一个常数,当超过某一值时,应变释放系数随着形状改变比能参数的增加成线性变化. 故以形状改变比能参数为变量对应变释放系数进行修正,能够达到较为理想的修正效果.

(2) 盲孔法测量高残余应力时,应考虑孔边塑性变形引起的测量误差. 通过大标定试验对应变释放系数进行修正,得到的修正公式具有较好的修正效果;同时与有限元模拟的修正值进行对比,结果较为符合. 说明用有限元进行应变释放系数的塑性修正是可行的.

参考文献:

[1] Annual Book of ASTM Standard, ASTM Designation[S]: E837—81, 1993 (3).

[2] Nawwar A M, Melachlan K, Shewchuk J. A modified hole-drilling technique for determining residual stress in thin plate[J]. Experimental Mechanics, 1976, 16(6): 226—232.

[3] 赵海燕, 裴 怡, 史耀武, 等. 用小孔释放法测量焊接高残余应力时孔边塑性变形对测量精度的影响及修正方法[J]. 机械强度, 1996, 18(3): 17—20.
Zhao Haiyan, Pei Yi, Shi Yaowu, et al. The influence and correction to the measuring error of high welding residual stress when using hole-drifting method[J]. Journal of Mechanical Strength, 1996, 18(3): 17—20.

[4] 李广铎, 刘柏梁, 李本远. 孔边塑性变形对测定焊接残余应力精度的影响[J]. 焊接学报, 1986, 7(2): 87—93.
Li Guangduo, Liu Boliang, Li Benyuan. Influence of hole-side plastic deformation on the accuracy of residual welding stress measurement[J]. Transactions of the China Welding Institution, 1986, 7(2): 87—93.

[5] 陆才善, 侯德门. 高残余应力钻孔法测量[J]. 机械强度, 1988, 10(1): 34—38.
Lu Caishan, Hou Demen. Measuring high level residual stress by hole drilling method[J]. Journal of Mechanical Strength, 1988, 10(1): 34—38.

[6] 刘一华, 贺赟晖, 詹春晓, 等. 盲孔法中释放系数的数值计算方法[J]. 机械强度, 2008, 30(1): 033—036.
Liu Yihua, He Yunhui, Zhan Chunxiao, et al. Numerical method for calculation of release coefficients in blind hole method[J]. Journal of Mechanical Strength, 2008, 30(1): 034—036.

作者简介: 马雯波, 男, 1986年出生, 硕士研究生. 主要从事焊接残余应力和锅炉压力容器方面的科研工作. 发表论文 2篇. Email: mawenbo3@163.com

通讯作者: 刘吉普, 男, 教授. Email: liujipu@yahoo.com.cn

Science and Technology, Nanjing University of Aeronautics and Astronautics, Nanjing 210016, China; 2. College of Mechanical Engineering, Huaiyin Institute of Technology, Huaian 223001, China; 3. Zhejiang Xinrui Welding Material Co., Ltd., Shengzhou 312000, China). p 93−96

Abstract: Cu/Al dissimilar metals were brazed with Zn-Al filler metals by torch-brazing technology, and the effects of Al on the spreadability and microstructure of Zn-Al filler metal were investigated separately. Moreover, the strength and microstructure of the brazed joint were also studied. Results indicate that the strength of the brazed joints achieves the optimum status when the Al content of filler metals is 15%. SEM and EDS are used to study the microstructure and phase constitution of the filler metals and brazed joints respectively. Experimental results show the microstructures of brazed joints are mainly consisted of Zn-based solid solution when Al content is low. However, $CuAl_2$ intermetallic compounds can form in the brazing seam region with increase of Al content. When Al content is 22 wt.%, $CuAl_2$ intermetallic compounds become coarse, and the strength of brazed joint decreases.

Key words: Cu/Al brazed joint; mechanical property; microstructure; $CuAl_2$ phase

FEM simulation of calibration on strain release coefficients in blind hole method

MA Wenbo[1,2], CHEN Shuguang, LIU Huijiong, LIN Wen[2], SHEN Yulong, LIU Jipu[1] (1. School of Mechanical Engineering, Xiangtan University, Xiangtan 411105, China; 2. Hunan Special Equipment Inspection & Testing Center, Changsha 410000, China). p 97−100

Abstract: The significant error of the measuring result may arise when measuring welding residual stress by means of the blind hole method. Because the stress around the hole exceed the yield limit, the plastic deformation induces plastic strain. Therefore, based on the principle of the calibration experiment, the strain release coefficients A and B of the steel Q345R are determined. According to the energy parameter S, the strain release coefficient A and B can be revised by the variation formulas, by this method, the result of measuring high residual stress can be more accurate. Based on the strength theory, the strain release coefficients A and B of steel Q345R, which were numerically calculated by the finite element method (FEM), coincide well with the calibration experiment results. So the FEM determination of the strain release coefficients A and B is viable.

Key words: blind-hole method; welding residual stress; strain release coefficient; calibration experiment; finite element method

Effects of CO_2 laser beam action on temperature of TIG arc

WU Shikai, XIAO Rongshi (Institute of Laser Engineering, Beijing University of Technology, Beijing 100124, China). p 101−104

Abstract: In order to understand the effects of a vertically incident CO_2 laser beam on the tungsten-inert gas (TIG) arc characteristics, the spectra of the arc plasma with the action of a vertically incident laser beam are analyzed. The electron temperature of the arc plasma is calculated by the boltzmann plot method. The results show that the electron temperature of the arc plasma with the action of CO_2 laser beam radiation is increased between the laser acting position and anode zone. The influences of laser power, arc current and laser acted position on electron temperature are also studied. The charges in electron temperature indicate that the inverse bremsstrahlung absorption of laser energy is the dominant factor influencing the electron temperature of TIG arc plasma with the action of CO_2 laser beam.

Key words: CO_2 laser; TIG arc; spectral diagnosis; electron temperature; inverse bremsstrahlung absorption

Joint performance of duplex stainless steel 2205 by laser-MIG hybrid welding

WANG Zhiyu[1], XU Haigang, WU Weiwei, ZHANG Lijuan[2] (1. Research and Development Center, Baoshan Iron & Steel Co., Ltd., Shanghai 201900, China; 2. TWI, Cambridge CB21 6AL, UK). p 105−108

Abstract: Phase ratio in weld metal and heat affected zone of duplex stainless steel will be unbalanced and joint properties deteriorated because of fast cooling rate after welding by conventional high energy density beam, so the duplex stainless steel 2205 is welded by using laser-MIG hybrid welding method, and the microstructure, mechanical property and corrosive property of welded joint are analyzed. The results show that the phase ratio of ferrite in weld metal and heat-affected zone is controlled between 40%−70%, the microhardness and tensile strength of the joint are higher than those of base metal, the impact toughness of weld metal, fusion line and heat-affected zone at −40 ℃ is 73, 205, 190 J/cm², respectively, and the critical pitting temperature (CPT) of weld bead is 49 ℃, near the same as that of base metal. So the good joint performance of duplex stainless steel 2205 can be obtained by laser-MIG hybrid welding.

Key words: duplex stainless steel; hybrid welding; microstructure; mechanical property; critical pitting temperature

Microstructures and corrosion-resistant performance of Al twin wire MIG welded joint

RUAN Ye[1], QIU Xiaoming, GONG Wenbiao[2], ZHAO Shihang, SUN Daqian[1] (1. School of Materials Science and Engineering, Jilin University, Changchun 130025, China; 2. School of Materials Science and Engineering, Changchun University of Technology, Changchun 130012, China). p 109−112

Abstract: Microstructures and corrosion-resistant performance of 6082-T6 Al twin wire MIG welded joint are studied by SEM and XRD technology. Experiments show that the welded seam is composed of a lot of α-Al, α-Al + Mg_2Si and a few Mg_2Si, moreover, Mg_2Si largely presents in the grain boundary. Corrosion-resistant performance is studied by measuring the potentiodynamic polarization curves and corrosion surface morphologies of twin wire MIG welded joint, and the results show that corrosion-resistant performance of the matrix is better than that of the weld seam, and precipitated Mg_2Si decreases the corrosion-resistant performance of the weld seam.

Key words: 6082-T6 Al alloy; twin wire MIG; microstructures; corrosion